ISSN 1063-7745, Crystallography Reports, 2018, Vol. 63, No. 4, pp. 614–620. © Pleiades Publishing, Inc., 2018.
Original Russian Text © D.N. Karimov, V.V. Grebenev, A.G. Ivanova, K.V. Khaydukov, A.A. Sidorov, E.A. Kulchenkov, P.A. Popov, B.P. Sobolev, 2018, published in Kristallografiya, 2018, Vol. 63, No. 4, pp. 586–592.

PHYSICAL PROPERTIES OF CRYSTALS

Thermal Expansion of EuF_{2+x} Single Crystals and Their Thermal Stability

D. N. Karimov[a,*], V. V. Grebenev[a], A. G. Ivanova[a], K. V. Khaydukov[a], A. A. Sidorov[b], E. A. Kulchenkov[b], P. A. Popov[b,], and B. P. Sobolev[a]**

[a] *Shubnikov Institute of Crystallography, Federal Scientific Research Centre "Crystallography and Photonics," Russian Academy of Sciences, Moscow, 119333 Russia*

[b] *Petrovskii Bryansk State University, Bryansk, 241036 Russia*

**e-mail: dnkarimov@gmail.com*

***e-mail: tfbgubry@mail.ru*

Received February 13, 2018

Abstract—Thermal expansion of an $EuF_{2.136}$ nonstoichiometric crystal with the fluorite structure type ($Eu^{2+}_{0.864}Eu^{3+}_{0.136}F_{2.136}$, lattice parameter 5.82171(5) Å) has been experimentally investigated in the temperature range of 9–500 K. The coefficient of thermal expansion is $\alpha = 15.8 \times 10^{-6}$ K^{-1} at $T = 300$ K. The observed anomalies in the behavior of the coefficient of thermal expansion at $T > 400$ K are related to the oxidation processes with partition of Eu^{2+} ions. It is established by differential scanning calorimetry that the onset temperature of EuF_{2+x} oxidation in air is 430 K and that this process occurs in three stages. X-ray diffraction analysis shows that the oxidation is accompanied by the formation of a phase mixture based on two modifications of the $Eu^{3+}_{1-y}Eu^{2+}_{y}F_{3-y}$ solid solution with the structure types of tysonite (LaF_3), orthorhombic β-YF_3 phase, and europium oxyfluorides of variable composition $EuO_{1-x}F_{1+2x}$, with dominance of the latter.

DOI: 10.1134/S1063774518040107

INTRODUCTION

Although nonstoichiometric $Eu^{2+}_{1-x}Eu^{3+}_{x}F_{2+x}$ crystals (EuF_{2+x}) with the fluorite structure type (sp. gr. $Fm\bar{3}m$) containing europium cations in different oxidation states are promising polyfunctional crystalline materials [1–5], they have been poorly studied to date.

To use crystals in practice, one should know the thermal dependences of their properties (in particular, coefficient of thermal expansion (CTE), one of the fundamental characteristics of a solid matter), because most applications of crystals imply thermomechanical impact.

The unusual character of the temperature dependence of linear CTE $\alpha(T)$ for an EuF_2 crystal in the temperature range $T = 298$–473 K was established in [6]. The anomaly in the behavior of lattice parameter $a(T)$ of an EuF_2 crystal of nominal composition in the region $T > 413$ K was revealed in [7]; however, the observed deviations in the monotonicity of the dependences were multidirectional. Proceeding from the lattice parameter $a = 5.8201$ Å for $T = 300$ K, obtained in [7] for an EuF_2 crystal of nominal composition, its real composition determined from the concentration dependence $a(x)$ of the EuF_{2+x} solid solution [8] corresponds to $x \sim 0.15$, while there are no data on the crystals investigated in [6].

The main purpose of this work was to experimentally investigate the thermal expansion of $EuF_{2.136}$ crystals grown from melt in a wide temperature range and study the thermal and chemical (Eu^{2+} oxidation) stabilities of EuF_{2+x} crystals by the methods of synchronous thermal analysis (STA)—differential scanning calorimetry and thermogravimetry (DSC–TG)—and X-ray diffraction (XRD) analysis.

EXPERIMENTAL

The samples for measuring CTE were pressed pellets prepared from a powdered $EuF_{2.136}$ crystal with a lattice parameter $a = 5.82171(5)$ Å (at room temperature), which was grown from a melt by the Bridgman technique [1, 9]. The adhesive component was alcohol solution of BF-2 glue.

Interplanar spacings d were measured from the changes in the position of X-ray diffraction maxima on an upgraded DRON-3 X-ray diffractometer device ($\lambda = 2.28962$ Å, CrK_α radiation) using an original low-temperature evacuated chamber [10] (Fig. 1) and an automatic system of setting and maintaining tempera-

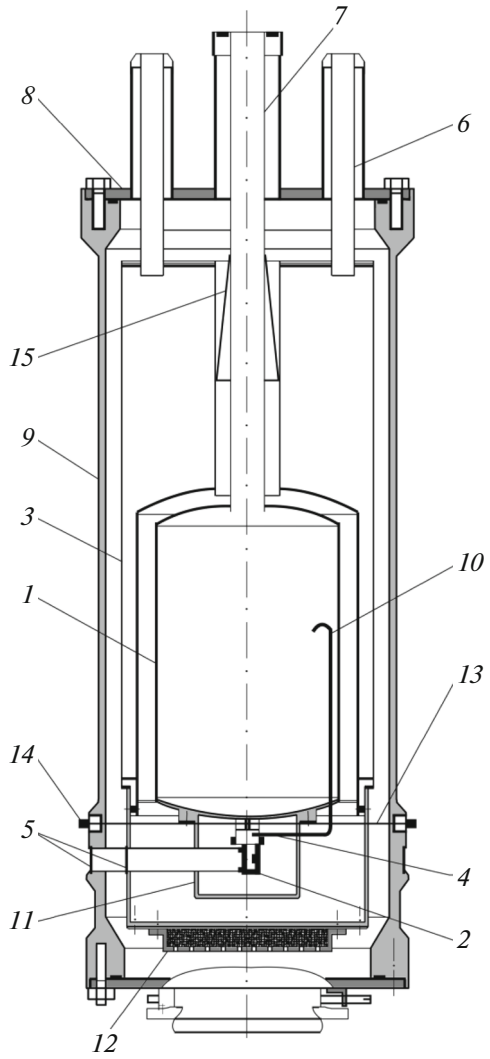

Fig. 1. Schematic of the low-temperature X-ray chamber: (*1*) liquid helium/nitrogen vessel, (*2*) sample holder, (*3*) nitrogen jacket, (*4*) thermal gas key, (*5*) beryllium windows, (*6*, *7*) thin-wall stainless tubes, (*8*) chamber flange, (*9*) chamber body, (*10*) stainless capillary, (*11*) helium radiation screen, (*12*) adsorption vacuum pump, (*13*) supporting string, (*14*) supporting string holder, and (*15*) heat sink.

ture with a stabilization error of ±0.1 K. The coolants were liquid helium and nitrogen. The temperature measurement ranges were T = 9–153 and 77–313 K, respectively. High-temperature (T = 299–500 K) measurements of the interplanar spacings were carried out in air using a heater with a stabilization error of ±0.3 K. The measurements were performed near the diffraction angle of 2θ ~ 149° (the Bragg reflection from the (422) crystallographic plane). The sample was heated stepwise with a step varying from ΔT = 2 K in the region of liquid-helium temperatures to ΔT = 20 K in the high-temperature region. The shape of the Bragg reflections depended on the measurement temperature. The most significant distortions of the reflections were observed in the high-temperature region. The error in determining of the interplanar spacing, calculated from the Bragg equation, did not exceed $\pm 6 \times 10^{-5}$ Å in the range $T < 299$ K and $\pm 4 \times 10^{-4}$ Å in the high-temperature region.

The experimental array of points $a(T)$ was divided into four overlapping regions, which were approximated by third-order polynomials. The linear CTE values were calculated from the formula $\alpha = \frac{da}{dT}\frac{1}{a}$. The obtained $\alpha(T)$ values were also approximated.

The chemical transformations in the EuF_{2+x} samples (x ~ 0.1, a = 5.8261(1) Å and x ~ 0.136, a = 5.8217(5) Å) were studied using an STA NETZSCH 449 F1 synchronous thermal analyzer in flows of humid argon and air (relative humidity 40% at 298 K) in the range of 300–700 K with a heating rate of 5 K/min; Pt/Rh crucibles were used. The error in measuring the mass did not exceed ±0.1 μg. Analyses were carried out on polycrystalline EuF_{2+x} powders with a particle size of ~10 μm.

The heat treatment of fine-grained powders was performed in air (under low-humidity conditions), in glassy carbon crucibles (SU-2000 grade) in a muffle furnace, in the temperature range of 473–723 K for 20–24 h. The temperature was maintained constant with an error of ±2 K.

XRD analysis of the heat-treatment products was performed with a Rigaku MiniFlex 600 powder X-ray diffractometer (CuK_α radiation) in the range 2θ = 10°–100°. The phases were identified using the ICDD PDF-2 (2014) database. The unit-cell parameters and quantitative phase ratios were calculated by Rietveld full-profile analysis using the High Score Plus software (PANanalytical, the Netherlands).

Luminescence spectra in the visible spectral range were measured with a FluoroLog-3 spectrofluorimeter (Horiba Jobin Yvon) at room temperature.

RESULTS AND DISCUSSION

Thermal Expansion of Crystals

The results of studying the temperature dependence of lattice parameter $a(T)$ of the $EuF_{2.136}$ sample are presented in Fig. 2 (curve *1*). The results of measuring $a(T)$ for EuF_2 [7] are also shown for comparison (curve *2*). One can see that the obtained dependence $a(T)$ monotonically increases in the temperature range T < 435 K, simbatically with the data of [7]; however, the monotonicity of the dependence $a(T)$ is violated at higher temperatures.

The results of calculating the dependence $\alpha(T)$ for $EuF_{2.136}$ in the range T = 20–430 K are presented in Fig. 2 (curve *3*). The values of $\alpha(T)$ for an EuF_2 crystal from [6] are also shown for comparison (curve *4*). The data obtained are summarized in Table 1.

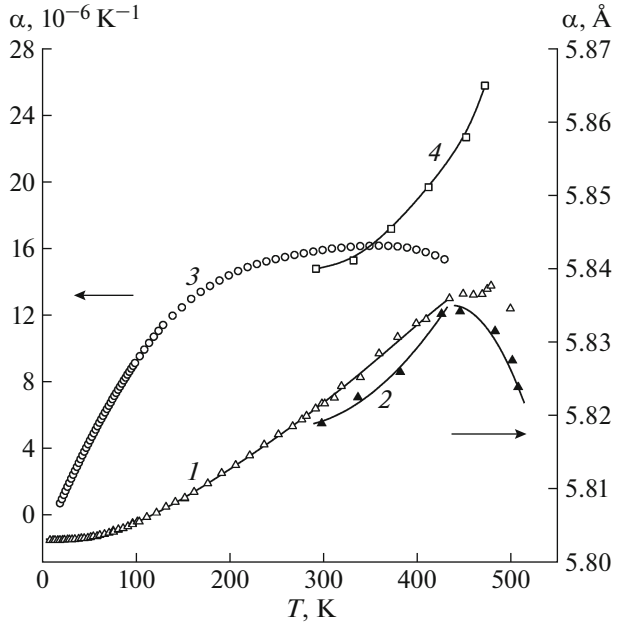

Fig. 2. Temperature dependences of the (*1*) $EuF_{2.136}$ lattice parameter in comparison with the (*2*) data of [7] for EuF_2 and (*3*) CTE of the $EuF_{2.136}$ crystal in comparison with the (*4*) data of [6].

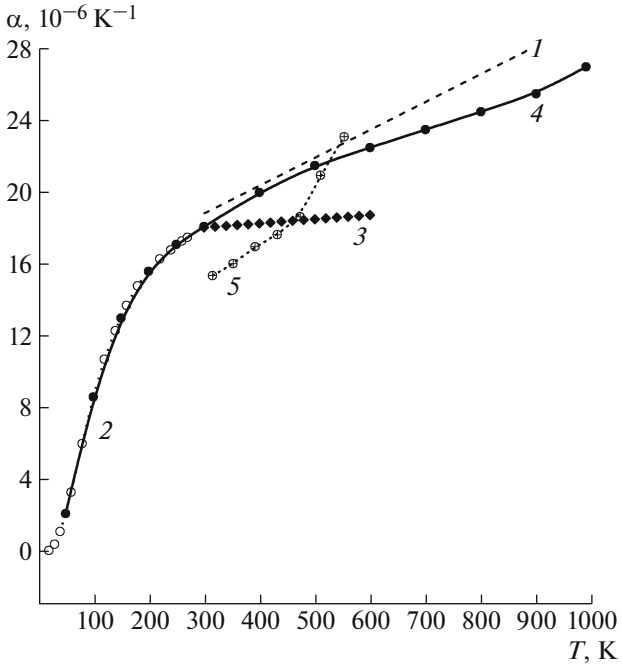

Fig. 3. Temperature dependence of the CTE of SrF_2 crystals according to the data of (*1*) [11], (*2*) [12], (*3*) [13], (*4*) [14], and (*5*) [15].

For comparison, Fig. 3 shows the dependence $\alpha(T)$ for crystalline SrF_2 [11–15], the lattice parameter of which is most close to that of EuF_2 among fluorides of alkaline-earth elements (a = 5.8003(6) Å [16]). It can be seen in Fig. 3 that the data obtained by different authors differ significantly, especially in the high-temperature region. Notably, both absolute CTE values and their temperature dependences $d\alpha/dT$ differ. A possible reason is the difference in the measurement methods, data processing techniques, and sample states (for example, the presence of mechanical stress, etc.). The measurements performed in [6, 12] were characterized by a significant increase in the dependence $\alpha(T)$, which is likely a drawback of the used experimental technique (curve *4* in Fig. 2 and curve *5* Fig. 3).

A comparison of the CTE data for the $EuF_{2.136}$ (Fig. 2, curve *3*) and SrF_2 (Fig. 3, curve *2*) crystals shows that the dependence $\alpha(T)$ for $EuF_{2.136}$ increases more rapidly at low temperatures and its slope decreases more rapidly upon heating. At $T > 200$ K, the linear CTE values of the $EuF_{2.136}$ crystals are smaller than those of the SrF_2 crystals by 20% on average. The CTEs of $EuF_{2.136}$ are close to the corresponding values for isotypic $Ca_{1-x}R_xF_{2+x}$ crystals (R = Y or Yb) investigated in [17] using a similar technique; they differ only slightly from the corresponding values for the initial fluorite CaF_2 matrix.

The observed change in the monotonic run of the dependence $\alpha(T)$ for $EuF_{2.136}$ at $T > 400$ K can be related to both the presence of mechanical stress in the crystal under study and the change in the oxidation state of Eu^{2+} ions in the samples upon heating in air. These factors could manifest themselves in a strong distortion of the Bragg reflections and, correspondingly, in the measurement results.

The thermal stability of EuF_{2+x} crystals was experimentally studied by the STA and XRD methods to establish the physical nature of the observed anomalous behavior of the dependence $\alpha(T)$ for $EuF_{2.136}$ in the temperature region under consideration.

The available information about the stages of EuF_{2+x} oxidation is contradictory, which is due to the phase variety of europium fluorides and oxyfluorides of constant and variable compositions [18]. According

Table 1. Values of the unit-cell parameter and linear CTE of the $EuF_{2.136}$ crystal for different temperatures

T, K	a, Å	α, 10^{-6} K^{-1}
10	5.8032(5)	–
20	5.8031(9)	0.62
50	5.8035(2)	4.2
100	5.8055(3)	9.0
200	5.8127(2)	14.3
300	5.8217(5)	15.8
400	5.832(3)	15.9

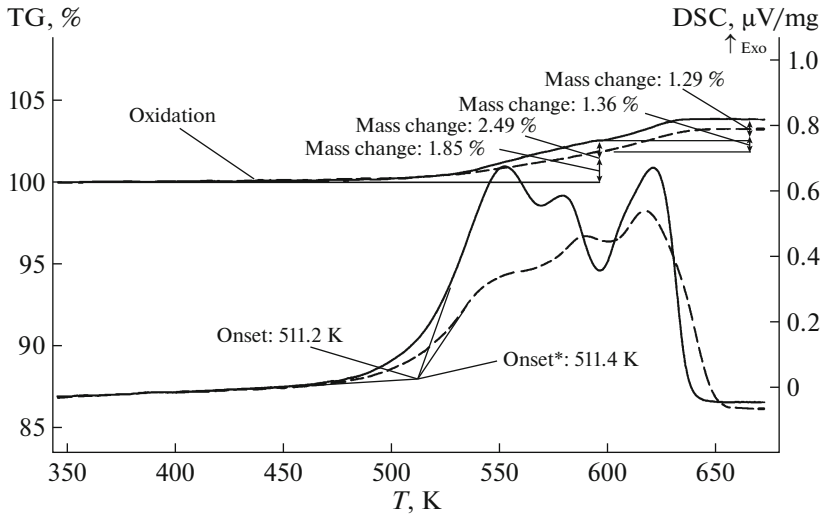

Fig. 4. Thermograms of the polycrystalline EuF_{2+x} samples with x = (solid line) 0.1 and (dotted line) 0.136.

to the data of [7], EuF_2 samples undergo oxidation with the formation of Eu_2O_3 phase upon heating in air ($T > 413$ K).

According to the data of [19], the process of EuF_2 oxidation in air occurs in one stage (exothermic effect at $T \sim 583$ K), with the formation of a single product: oxyfluoride Eu_2OF_4 ($EuO_{0.5}F_2$) with a trigonally distorted fluorite structure. For europium fluorides of variable composition, EuF_{2+x} ($0 < x < 0.5$), the oxidation process depends on the ratio of Eu^{2+} and Eu^{3+} ions in the sample under study and occurs in two stages:

$$EuF_{2+x} \xrightarrow{T=493-573\ \mathrm{K},\ O_2} 2xEuF_{2.5} + ((1-2x)/2)Eu_2OF_4;$$

further oxidation of cubic $EuF_{2.5}$ ($a = 5.760(5)$ Å) follows the scheme

$$2EuF_{2.5} \xrightarrow{T=573-673\ \mathrm{K},\ O_2} (1/2)Eu_2OF_4 + EuF_3,$$

where the Eu_2OF_4 and orthorhombic EuF_3 phases are stable up to $T \sim 873$ K.

Pyrohydrolysis of EuF_3 in air can be presented as a sequence of the following transformations:

$$EuF_3 \xrightarrow{T=1173-1213\ \mathrm{K}} Eu_2OF_4 \xrightarrow{T=1213-1273\ \mathrm{K}} Eu_4O_3F_6 \xrightarrow{T=1273-1313\ \mathrm{K}} EuO_{1-x}F_{1+2x}\ (0.08 > x \geq 0) \xrightarrow{T>1313\ \mathrm{K}} Eu_2O_3,$$

where oxyfluorides Eu_2OF_4, $Eu_4O_3F_6$, and $EuO_{1-x}F_{1+2x}$ have the trigonal, tetragonal, and orthorhombic symmetry, respectively [20].

The process of oxidation of $EuF_{2.16}$ samples (a = 5.814 Å) in air was investigated in [5]. It was shown that the compound is stable up to $T \sim 473$ K, and further heating leads to two-stage $EuF_{2.16}$ oxidation to oxyfluoride with the $EuO_{0.66}F_{1.67}$ composition ($Eu_3O_2F_5$), which is crystallized into the monoclinic (orthorhombic, according to the data of [21]) system.

Our investigations show that crystalline EuF_{2+x} samples ($x \sim 0.1$ or 0.136) are stable in a humid-argon flow up to $T = 623$ K, and the sample masses remain constant within an error of 0.01%. Concerning oxidation in humid air, fluorides EuF_{2+x} are unstable, and their oxidation is described by a multistep mechanism.

One can distinguish three oxidation stages for EuF_{2+x} samples in the thermograms presented in Fig. 4, which almost coincide for different x.

The first two stages (maxima at $T = 553$ and 580 K for $EuF_{2.136}$) lead to an increase in the mass Δm = 2.49%, and the last stage ($T = 621$ K) corresponds to the increase $\Delta m = 1.29\%$. The $EuF_{2.1}$ sample behaves similarly. Since neither composition is stoichiometric, it does not seem possible to compare the increase in mass with theoretically possible values and determine the probability of a particular version of EuF_{2+x} oxidation reaction.

An essential conclusion, which was not reported in [5, 19], was drawn from the analysis of the thermogravimetric curve behavior. The onset of the oxidation process, which is determined as a point of intersection of the tangents from the inflection point of the DSC signal peak and the baseline, corresponds to the onset of the oxidation process with a constant rate; i.e., it is a kinetic quantity and depends on the sample heating rate, because the DSC technique is a dynamic measurement method. The oxidation process is determined by not only kinetics but also thermodynamics. The point of deviation of the thermogravimetric curve from the horizontal line is indicated in Fig. 4; it corresponds to the beginning of the sample mass increase.

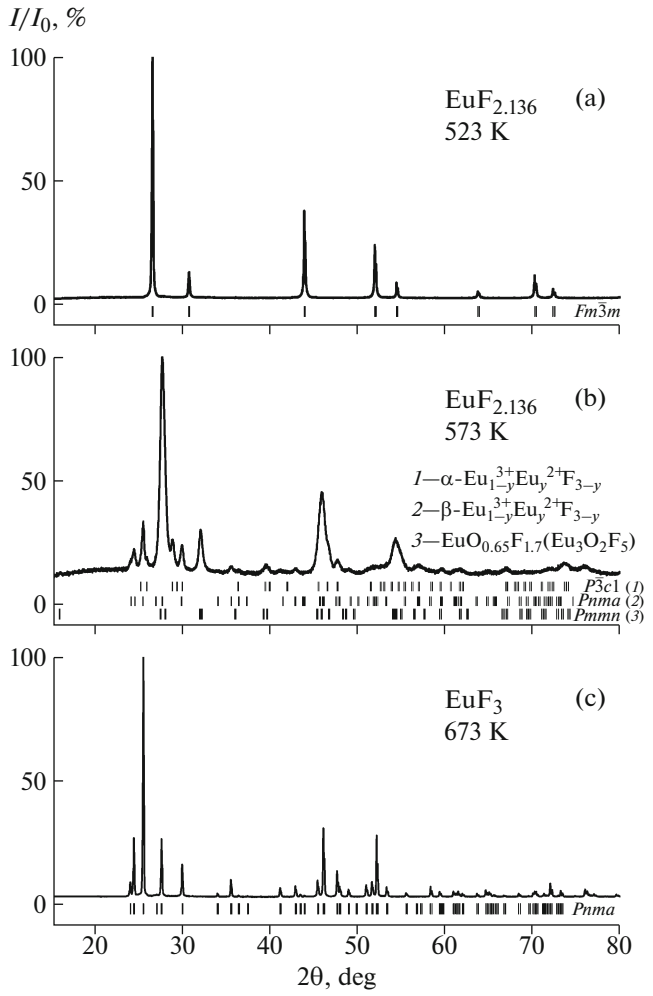

Fig. 5. X-ray diffraction patterns of the products of thermal treatment of (a, b) $EuF_{2.136}$ powder in air at T = (a) 523 and (b) 573 K and (c) EuF_3 powder at T = 673 K. The Bragg reflections for the phases of the noted space groups are shown.

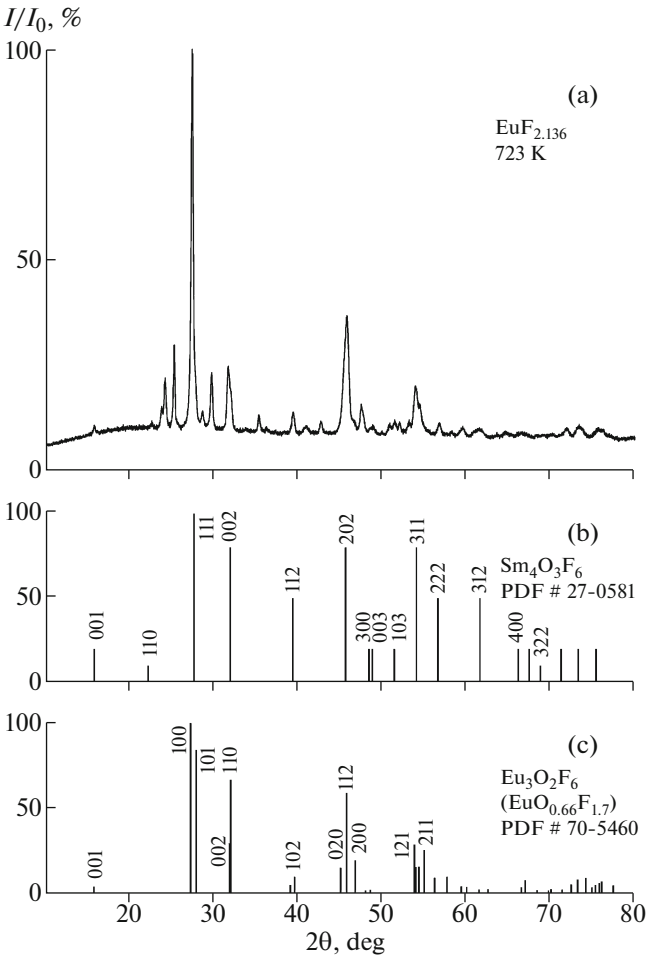

Fig. 6. X-ray diffraction patterns of the products of thermal treatment of the (a) $EuF_{2.136}$ powder in air at T = 723 K, (b) tetragonal oxyfluoride $Eu_4O_3F_6$ [24], and (c) orthorhombic oxyfluoride $Eu_3O_2F_5$ [21].

Thus, the onset temperature of the EuF_{2+x} oxidation process upon heating with a constant rate of 5 K/min was found to be T_o = 430 K, which corresponds to the onset temperature of the anomalous behavior of the dependence $a(T)$ for the EuF_{2+x} crystal (Fig. 2, curve *1*) but is below the values reported in [5].

The XRD results for the $EuF_{2.136}$ powders annealed at different temperatures are shown in Figs. 5 and 6. The fluorite phase, which is stable at T = 523 K (Fig. 5a), disappears completely upon further heating. No formation of the limiting (according to the data of [19]) fluorite $EuF_{2.5}$ solid solution was recorded.

A three-phase mixture is observed at T = 573 K (Fig. 5b); it consists of orthorhombic (monoclinic, according to the data of [18]) oxyfluoride $EuO_{1-x}F_{1+2x}$ ($x \sim 0.33$–0.35, i.e., $Eu_3O_2F_5 = EuF_3 \cdot 2EuOF$) [20, 21], which dominates, and two modifications based on the $Eu^{3+}_{1-y}Eu^{2+}_yF_{3-y}$ solid solution with the tysonite (LaF_3) and orthorhombic β-YF_3 structure types (Table 2). The possibility of stabilizing the high-temperature tysonite phase (sp. gr. $P\bar{3}c1$) at room temperature due to the formation of $Eu^{3+}_{1-y}Eu^{2+}_yF_{3-y}$ solid solution was demonstrated in [22].

For comparison, Fig. 5c shows an X-ray diffraction pattern of EuF_3 sample annealed at T = 673 K. After the annealing, EuF_3 remains single-phase (sp. gr. *Pnma*, a = 6.6193(5) Å, b = 7.0175(5) Å, c = 4.3958(5) Å), and its pyrohydrolysis onset temperature in humid air is T = 938 K [23].

The increase in the annealing temperature for $EuF_{2.136}$ samples to T = 723 K (Fig. 6) is accompanied by further oxidation of europium oxyfluoride according to the scheme

Table 2. Phase composition of the $EuF_{2.136}$ sample oxidation products at $T = 573$ K

Phase	Sp. gr.	Lattice parameters, Å	Phase ratio, wt %
$EuO_{1-x}F_{1+2x}$ ($x = 0.33$–0.35), $Eu_3O_2F_5$	*Pmmn*	$a = 3.9596(1)$ $b = 3.9936(1)$ $c = 5.5471(1)$	64
$Eu^{3+}_{1-y}Eu^{2+}_{y}F_{3-y}$ (β phase)	*Pnma*	$a = 6.6461(1)$ $b = 7.0100(1)$ $c = 4.3746(1)$	26
$Eu^{3+}_{1-y}Eu^{2+}_{y}F_{3-y}$ (α phase)	$P\bar{3}c1$	$a = 6.9307(1)$ $c = 7.0492(1)$	10

$$3Eu_3O_2F_5(EuO_{0.66}F_{1.7}) \rightarrow 2Eu_4O_3F_6(EuO_{0.75}F_{1.5}) + EuF_3.$$

This process determines the third high-temperature stage in the DSC thermogram (Fig. 4). The $Eu_4O_3F_6$ phase ($EuO_{0.75}F_{1.5}$), isostructural with $Sm_4O_3F_6$, has a tetragonal symmetry with the lattice parameters $a = 5.623(2)$ Å and $c = 5.574(3)$ Å [20, 24]. For comparison, Fig. 6 shows the X-ray diffraction patterns of $Sm_4O_3F_6$ [24] and $Eu_3O_2F_5$ [21]. The X-ray diffraction patterns for the $EuF_{2.1}$ samples barely differ from those for the $EuF_{2.136}$ samples.

The $EuF_{2.136}$ samples annealed at $T = 723$ K remain three-phase (Fig. 6). As compared with the X-ray diffraction pattern of the samples annealed at $T = 573$ K (Fig. 5b), an increase in the annealing temperature reduces significantly the relative intensity of reflections of the phase based on the high-temperature

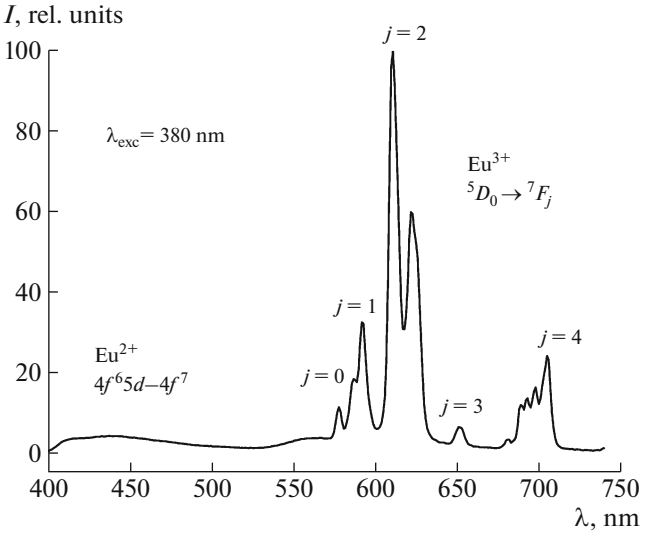

Fig. 7. Luminescence spectrum of the $EuF_{2.136}$ sample after thermal treatment ($T = 723$ K). The excitation wavelength is $\lambda_{exc} = 380$ nm.

α-modification of EuF_3 (sp. gr. $P\bar{3}c1$, $a = 6.9128(1)$ Å, $c = 7.0286(1)$ Å), while the intensity of reflections of the orthorhombic β-phase of EuF_3 (sp. gr. *Pnma*, $a = 6.6308(1)$ Å, $b = 7.0166(1)$ Å, $c = 4.3927(1)$ Å) is almost doubled, and its lattice parameters approach the values for stoichiometric EuF_3 [21]. Thus, the EuF_2 fraction in the $Eu^{3+}_{1-y}Eu^{2+}_{y}F_{3-y}$ solid solution decreases for both modifications during thermal treatment (at $T = 723$ K); however, some amount of Eu^{2+} ions is retained, and their presence can be revealed by spectroscopic methods.

In the luminescence spectrum of the $EuF_{2.136}$ sample annealed at $T = 723$ K, a wide $5d$–$4f$ band in the range $\lambda = 400$–470 nm, typical of Eu^{2+} ions, is observed against the background of strong bands in the wavelength range $\lambda > 570$ nm, which are due to Eu^{3+} ions (Fig. 7). The presence of Eu^{2+} ions in the products of EuF_{2+x} oxidation in air was also shown in [5].

It is not inconceivable that oxygen isomorphically substitutes for fluorine in the anion sublattice during thermal treatment, and the EuF_3-based solid solution has a more complex composition: $Eu^{3+}_{1-y}Eu^{2+}_{y}O_zF_{3-y-2z}$. In this case, phases with cation ($Eu^{2+} \rightarrow Eu^{3+} + F^{1-}$) and anion ($2F^{1-} \rightarrow O^{2-}$) nonstoichiometries are formed, which should be checked experimentally. A combination of two types of deviation from stoichiometry in crystals with the fluorite structure type will make it possible to extend the range of new materials with adjustable properties.

CONCLUSIONS

It was established that thermal expansion of an $EuF_{2.136}$ crystal in the temperature range of 9–400 K is typical of crystals with the fluorite structure. The linear CTE is $\alpha = 15.8 \times 10^{-6}$ K^{-1} at $T = 300$ K. At $T > 200$ K, the $\alpha(T)$ values of $EuF_{2.136}$ crystals are smaller than those of SrF_2 crystals by 20% on average. It was shown that violation of the monotonic behavior of the CTE dependence for the crystals under study in the range $T > 430$ K is related to the processes of EuF_{2+x} oxidation in air and occurs in three stages. The XRD analysis showed that EuF_{2+x} samples are oxidized upon heating with the formation of phases based on two modifications of the $Eu^{3+}_{1-y}Eu^{2+}_{y}F_{3-y}$ solid solution and europium oxyfluorides: $Eu_3O_2F_5$ at $T < 573$ K and $Eu_4O_3F_6$ at higher temperatures.

ACKNOWLEDGMENTS

This study was supported by the Russian Foundation for Basic Research, project nos. 16-03-00707 and 17-00-00118 KOMFI (growth of crystal samples), Federal Agency for Scientific Organizations (contract

no. 007-ГЗ/Ч3363/26 (investigation of the thermal stability of crystals), and the Ministry of Education and Science of the Russian Federation, state contract no. 3.8326.2017/8.9 (investigation of the thermal expansion of crystals). The experiments were performed using the equipment of the Collective-Use Centers of Bryansk State University and the Federal Scientific Research Centre "Crystallography and Photonics," Russian Academy of Sciences.

REFERENCES

1. B. P. Sobolev, T. M. Turkina, N. I. Sorokin, et al., Crystallogr. Rep. **55** (4), 657 (2010).
2. K. Lee, H. Muir, and E. Catalano, J. Appl. Phys. **36** (3), 1043 (1965).
3. J. C. Suits, B. E. Argyle, and M. T. Freiser, J. Appl. Phys. **37** (3), 1391 (1966).
4. D. N. Karimov, P. A. Popov, N. I. Sorokin, and B. P. Sobolev, Crystallogr. Rep. **62** (3), 411 (2017).
5. V. F. Zinchenko, O. G. Eremin, N. P. Efryushina, et al., Russ. J. Inorg. Chem. **50** (5), 676 (2005).
6. D. B. Sirdeshmukh and B. K. Rao, AIP Conf. Proc. **17**, 56 (1974).
7. K. A. Hussain and D. B. Sirdeshmukh, Cryst. Res. Technol. **28** (8), 147 (1993).
8. P. P. Fedorov and B. P. S obolev, Kristallografiya **37** (5), 1210 (1992).
9. P. A. Popov, N. V. Moiseev, D. N. Karimov, et al., Crystallogr. Rep. **60** (5), 740 (2015).
10. A. A. Sidorov, Candidate's Dissertation in Physics and Mathematics (Bryansk, 1987).
11. G. Kommichau, H. Neumann, W. Schmptz, and B. Schumann, Cryst. Res. Technol. **21** (12), 1583 (1986).
12. D. B. Sirdeshmukh and V. T. Deshpande, Indian J. Pure Appl. Phys. **2**, 405 (1964).
13. K. G. Subhadra, K. A. Hussain, W. Hussain, and D. B. Sirdeshmukh, J. Mater. Sci. Lett. **4** (6), 777 (1985).
14. A. C. Bailey and D. Yates, J. Phys. Soc. **91** (2), 390 (1967).
15. R. B. Roberts and G. K. White, J. Phys. C: Solid State Phys. **19** (36), 7167 (1986).
16. B. P. Sobolev, D. N. Karimov, S. N. Sul'yanov, and Z. I. Zhmurova, Crystallogr. Rep. **54** (1), 122 (2009).
17. A. A. Sidorov, P. A. Popov, S. V. Aksenov, et al., Inorg. Mater. **49** (5), 525 (2013).
18. B. Tanguy, M. Vlasse, and J. Porter, Rev. Chim. Miner. **10** (1–2), 63 (1973).
19. V. G. Bamburov, A. S. Vinogradova-Zhabrova, and V. A. Zhilyaev, Izv. Akad. Nauk SSSR, Ser. Neorg. Mater. **15** (10), 1779 (1979).
20. V. G. Bamburov, A. S. Vinogradova-Zhabrova, and N. D. Yakovleva, Izv. Akad. Nauk SSSR, Neorg. Mater. **9** (11), 1928 (1973).
21. J. P. Laval, A. Taoudi, and A. Abaouz, J. Solid State Chem. **157** (1), 134 (2001).
22. O. Greis and T. Petzel, Z. Anorg. Allg. Chem. **403** (1), 1 (1974).
23. S. Yonezawa, K. Jae-Ho, and M. Takashima, Solid State Sci. **4** (11–12), 1481 (2002).
24. K. Niihara and S. Yajima, Bull. Chem. Soc. Jpn. **44** (3), 643 (1971).

Translated by A. Sin'kov